RSC Advances

ROYAL SOCIETY OF CHEMISTRY

www.rsc.org/advances

RSC Advances

ARTICLE

Enhanced Oxidase/peroxidase-like Activities of Aptamer Conjugated MoS_2/PtCu Nanocomposites and Their Biosensing Application

Received 00th January 20xx,
Accepted 00th January 20xx

DOI: 10.1039/x0xx00000x

www.rsc.org/

Cui Qi†, Shuangfei Cai†, Xinhuan Wang, Jingying Li, Zheng Lian, Shanshan Sun, Rong Yang* and Chen Wang*

Hybrid composite materials are particularly useful and offer great opportunities for catalysis due to their multifunctionalities. Taking advantage of the high catalytic properties of bimetallic alloy nanoparticles, the large specific surface area and co-catalytic function of MoS_2 nanosheets, we prepare a novel MoS_2/PtCu nanocomposite with intrinsic high oxidase- and peroxidase-like activity. The preparation of MoS_2/PtCu nanocomposites does not require organic solvents or high temperature. The introduction of single-layer MoS_2 nanosheets not only improves porous PtCu nanoparticles with a fine dispersion, but also readily incorporates recognition elements. As a mimic oxidase, the independence of hydrogen peroxide shows good biocompatibility of MoS_2/PtCu for promising bioapplication. On the basis of oxidase-like activity, a novel colorimetric aptasensor (apt-MoS_2/PtCu) was developed and its application in colorimetric detection of cancer cells with different MUC1-protein densities was demonstrated. The as-prepared apt-MoS_2/PtCu shows good sensitivity and selectivity to targeting cells. The proposed strategy will facilitate the utilization of MoS_2-based nanocomposites with high oxidase/peroxidase activities in biotechnology, biocatalyst and *etc*.

Introduction

Owing to their unique properties, nanomaterials are attractive for high-efficiency catalysts and have been extensively studied during the past decade.[1, 2] In addition, nanomaterial-based enzyme mimics for colorimetric sensing have been applied in catalyst and bioassay. In comparison with natural enzymes, nanomaterial-based enzyme mimics have advantages of low costs, tunable catalytic activities, high stability against stringent reaction conditions, and ease of storage and treatment. The above robust physical or chemical properties make them promising candidates for colorimetric biosensing. Although a number of different nanomaterials were found with peroxidase- or oxidase-like activity, such as metal oxides,[3-8] carbon nanomaterials,[9-12] quantum dots,[13] noble metal complex,[14-16] and *etc.*, bimetallic nanoalloys have been demonstrated to exhibit improved catalytic performance because of the synergistic effect and the electronic effect.[17-22] Among the enzyme nanomimics, hybrid composite materials are particularly impressive and offer great opportunities for catalysis, since the combination of the respective properties of each component can achieve cooperatively enhanced performances. An increasing number of hybrid complexes with inorganic nanomaterials incorporated with different matrixes have been applied in catalyst.[23-26] Graphene-hemin composites,[27, 28] magnetic nanoparticle/CNT nanocomplexs,[29] GO-Fe_3O_4 nanocomposites[30] and noble metal-graphene hybrids[31, 32] have been proved to possess new and/or enhanced functionality that cannot be realized by either component alone. Therefore, to design and fabricate new multifunctional hybrid nanocomposites with high enzyme-like activity would be helpful to expand their applications in biomedical fields, such as optical biosensors and biocatalysts.

Considered as typical transition metal dichalcogenides and novel inorganic graphene analogues, MoS_2 has been widely studied and applied in catalyst, sensing, energy storage and electronic devices.[33-38] Besides the advantages of good chemical stability, low cost and environmental friendliness, porous MoS_2[39-42] with large specific surface area and catalytically active sites make them excellent candidates for capturing numerous biomolecules and provides

CAS Key Laboratory for Biological Effects of Nanomaterials and Nanosafety
CAS Center for Excellence in Nanoscience,
National Center for Nanoscience and Technology
Beijing, 100190, PR China
E-mail: yangr@nanoctr.cn; wangch@nanoctr.cn
† These authors are contributed equally to this work.
Electronic Supplementary Information (ESI) available. See DOI: 10.1039/x0xx00000x

promising opportunities for the development of the signal amplification strategy, which should be extremely attractive in the area of biosensors. Recently, it has been reported that MoS_2 nanosheets possessed an intrinsic peroxidase-like catalytic activity, which could catalyze the oxidation of 3,3,5,5-tetramethylbenzidine (TMB) in the presence of hydrogen peroxide (H_2O_2) to produce a blue color.[43, 44] The higher peroxidase-like activity with greater dispersity in aqueous solution of hemin/ MoS_2 nanosheet composites than hemin alone was also demonstrated.[45] Although a number of metal/ MoS_2 nanosheet hybrids were successfully synthesized,[46-49] their functionalities have not been well explored and very few biosensor applications have been reported.

Here, we designed a colorimetric biosensor based on aptamer-functionlizationed MoS_2/PtCu nanocomposites with high oxidase-like activity and demonstrated its biosensor application for the detection of cancer cells. The working principle is illustrated in Scheme 1.The synthesis of the MoS_2/PtCu nanocomposites is based on co-reduction of two metal salts by $NaBH_4$ on the surface of MoS_2 nanosheets. On the basis of the oxidase-like activity of MoS_2/PtCu nanocomposites and mucin 1 (MUC1) aptamers, selective binding apt-MoS_2/PtCu nanocomposites on the MUC1 overexpressed cells can convert the recognition process into quantitative colorimetric signal. This aptameric nanobiosensor has several advanced properties: (i) the preparation of MoS_2/PtCu nanocomposites were simple and rapid, without organic solvents or high temperature involved in the entire synthesis process; (ii) the formation of porous PtCu nanoalloys improved catalytic activity comparing with monometallic counterparts, and the porous nanostructure could also increase the contact with substrates; (iii) as the large surface area of single-layer MoS_2 nanosheets, large amounts of porous PtCu nanoparticles could be immobilized on it with a fine dispersion, resulted in remarkable amplification of the colorimetric signal and improved sensitivity. The large surface area could also improve immobilization sites for biological molecules (such as streptavidin); (iv) considering that most of the reported colorimetric biosensors need to go through complicated covalent modifications, our approach appeared to be simpler, and provided a general surface modification method through biotin-streptavidin interactions. By altering different recognition elements, one can develop different colorimetric biosensors with desired demands.

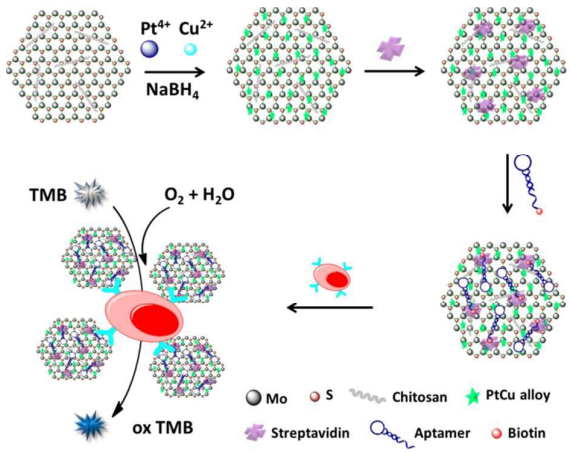

Scheme 1. Schematic representation of preparation of aptamer-functionlized MoS_2/PtCu colorimetric biosensor and its application for cancer-cell detection.

Results and discussion

Characteration of MoS_2/PtCu nanocomposites

The synthesis of MoS_2/PtCu nanocomposites was carried out without organic solvents or high temperature, and the obtained solution with good dispersity showed high stability against aggregation (Fig. S1). Transmission electron microscopy (TEM) image (Fig. 1a) revealed that porous PtCu nanoparticles had a homogeneous distribution on the surface of MoS_2 nanosheets with an average size less than 20 nm. The crystal structure of MoS_2/PtCu was characterized by X-ray diffraction (XRD). The four peaks appeared at 40.48, 46.86, 68.85 and 82.67 were coincidently located between Pt (reference code: 01-087-0646) and Cu (reference code: 01-085-1326), which could be indexed as the (111), (200), (220) and (311) planes of PtCu nanoalloys (Fig. 1c). High-resolution TEM (HR-TEM) and X-ray photoelectron spectroscopy (XPS) were further used to investigate the structure and element distributions of the MoS_2/PtCu nanocomposites. As shown in HR-TEM image (Fig. 1b), the lattice spacing of 0.19 nm and 0.22 nm are corresponding to the (200) plane and the (111) plane of PtCu nanoalloys respectively. The lattice spacing of 0.27 nm was corresponding to the (100) plane of MoS_2 nanosheets. Pt 4f peak, Cu 2p peak, Mo 3d peak and S 2p peak observed from XPS spectra (Fig. 1d and Fig. S2) were further confirmed the chemical state and the successful location of PtCu nanoalloys on MoS_2 nanosheets. The nanocomposite content was also analyzed by inductively coupled plasma optical emission spectroscopy (ICP-OES). The element concentrations of Pt and Cu were 0.117 mM and 0.016 mM respectively. The atomic ratio of Pt/Cu was 88:12.

Enzyme-like activity of MoS_2/PtCu nanocomposites

The oxidase-like activity of MoS_2/PtCu nanocomposites was investigated in catalysis of the substrates 2,2'-azino-bis(3-ethylbenzo-thiazoline-6-sulfonic acid) diammonium salt (ABTS), TMB and *o*-phenylenediamine (OPD), which had been used to demonstrate the oxidase- or peroxidase-like activities of other nanoparticles. As shown in Fig. 2a, MoS_2/PtCu nanocomposites could quickly catalyze the oxidation of the three common chromogenic substrates without H_2O_2 in phosphate buffer, producing the typical colors. The control experiment without MoS_2/PtCu nanocomposites showed negligible color variation. Moreover, after bubbling MoS_2/PtCu nanocomposite dispersion with nitrogen to remove dissolved oxygen, the reaction rate of TMB oxidation decreased dramatically (Fig. 2b). The above results indicated that MoS_2/PtCu nanocomposites exhibited an intrinsic oxidase-like activity, and the dissolved oxygen was the electron acceptors for the oxidation in the absence of H_2O_2.

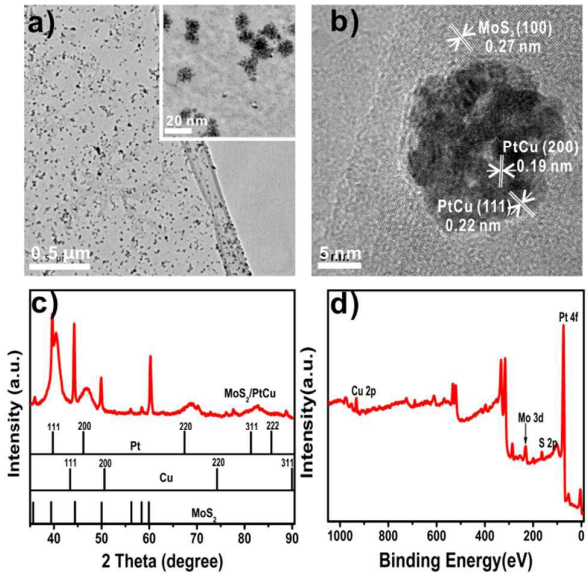

Fig. 1 (a) Representative TEM images, (b) HRTEM image, (c) XRD spectrum and (d) XPS spectrum of as-prepared MoS_2/PtCu nanocomposites.

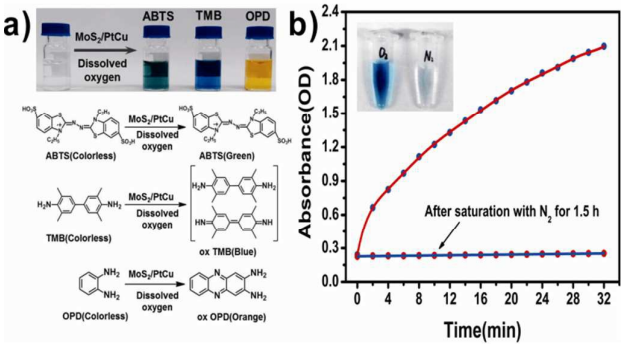

Fig. 2 (a) Color evolution of ABTS, TMB and OPD oxidation by dissolved oxygen using MoS_2/PtCu as catalysts. (b) The oxidase-like activity of MoS_2/PtCu before and after saturation with N_2.

In order to elucidate the catalytic reaction mechanism, it is essential to confirm the reactive oxygen species produced during the reaction. Terephthalic acid (TA) was reported as a fluorescence probe to confirm the generation of $^{\bullet}OH$, which formed highly fluorescent 2-hydroxy terephthalic acid after reacting with $^{\bullet}OH$.[50, 51] As shown in Fig. S3, the appearance of an emission peak at 425nm suggested the formation of the fluorescent products, which implied the production of $^{\bullet}OH$ after the interaction between MoS_2/PtCu nanocomposites and the dissolved oxygen in solution.

The influence of the composition for the catalytic activity was studied. As shown in Fig. 3, MoS_2/PtCu nanocomposites had the highest oxidase-like activity among different composites. MoS_2 nanosheets and MoS_2/Cu nanocomposites can't catalyze the oxidation of TMB by dissolved oxygen in water, suggesting that they didn't have oxidase-like activity. MoS_2/PtCu nanocomposites showed a level of activity 5 times higher than MoS_2/Pt nanocomposites at the same molar concentration. The above results indicated that the significant enhancement of the oxidase-like activity for MoS_2/PtCu nanocomposites might benefit from the bimetallic catalyst and the porous nanostructure of the PtCu nanoalloys. In addition, MoS_2/PtCu nanocomposites also had higher oxidase-like activity than the free PtCu nanoalloys, which suggested that MoS_2 nanosheets might also contribute to the high catalytic activity of the nanocomposites. For the high surface-to-volume ratios and strong surface adsorption capability, the substrates (such as TMB) could be absorbed onto MoS_2 nanosheets efficiently. Hence the substrates and the active sites of PtCu nanoalloys located on MoS_2 nanosheets were confined in a nanoscale region, which could enhance the catalytic activity of PtCu nanoalloys.

Furthermore, the peroxidase-like activity of MoS_2/PtCu nanocomposites was also studied. As shown in Fig. S4, after saturation with N_2 for 1.5 h to clear dissolved oxygen in buffer, MoS_2/PtCu nanocomposites could catalyze the oxidation of TMB in the presence of H_2O_2 to produce a blue color with maximum absorbance at 652 nm. In contrast, no obvious reaction occurred in the absence of MoS_2/PtCu, suggesting the peroxidase-like activity of

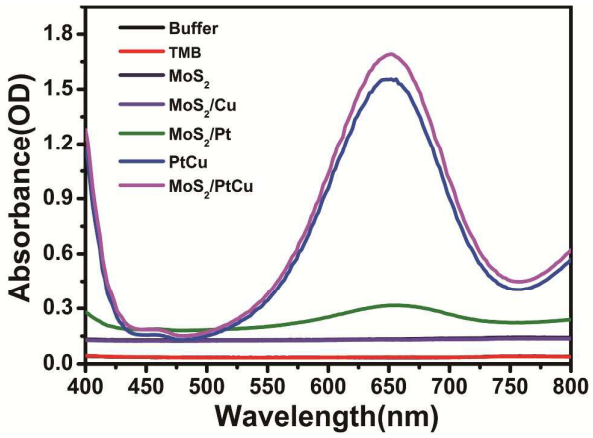

Fig. 3 The different oxidase-like activities of as-prepared nanomaterials (MoS_2, MoS_2/Cu, MoS_2/Pt, PtCu and MoS_2/PtCu).

the nanocomposites. For comparison between MoS_2/PtCu and HRP, Michaelis constant (K_m) and maximal reaction velocity (V_{max}) were obtained using Lineweaver-Burk plot and shown in Table S1. The apparent K_m value of MoS_2/PtCu with H_2O_2 as the substrate was higher than that for HRP, consistent with the observation that a higher H_2O_2 concentration was required to achieve maximal activity for MoS_2/PtCu. The apparent K_m value of the MoS_2/PtCu with TMB as the substrate was about two times lower than HRP, suggesting that MoS_2/PtCu has a higher affinity to TMB than HRP.

Production of aptamer-functionlizationed MoS_2/PtCu nanoconjugates and application in cancer-cell immunoassay

A number of folic acid-functionalized colormetric biosensors based on nanomaterial enzyme mimics have been reported to detect cancer cells.[15, 22, 28, 31, 32] However, most of the reported colorimetric biosensors need to go through complicated covalent modifications. Simple and facile preparation processes for colorimetric biosensors are highly desired. Here we introduce streptavidin to MoS_2/PtCu nanocomposites *via* physical adsorption, and then biotinylated aptamers were connected to surfaces. Our approach provides a general surface modification method through biotin-streptavidin interactions. The as-prepared nanocomposites were functionalized with a MUC1 aptamer termed S2.2 for cancer-cell detection.[52, 53] MUC1 is a large transmembrane glycoprotein of the mucin family overexpressed on the surface of most epithelial cancers (breast, lung, prostate and ovarian cancer, *etc.*).[52-55] MUC1 is an attractive protein target for cancer therapy. The extraordinary surface-area-to-mass ratio of MoS_2 nanosheets and the negatively charged surface of MoS_2/PtCu nanocomposites provide a convenient way for absorption of streptavidin without needs of other modifications. Biotinylated aptamer S2.2 was conjugated to MoS_2/PtCu via the adsorption of streptavidin on the nanocomposites. To maintain a high catalytic activity and acquire a good effect on cell recognition, the adsorbent concentrations of streptavidin and aptamer were optimized (Fig. S5). Then the conjugation of aptamer S2.2 to MoS_2/PtCu was confirmed by UV/Vis (Fig. S6), FTIR (Fig. S7) and zeta-potential (Table S2) measurements. In the UV/Vis spectra of the nanoconjugates, the new peak at 265 nm, which due to the overlap interference of spectrum peak at 260 nm for S2.2 aptamer and spectrum peak at 280 nm for streptavidin, suggested the formation of apt-MoS_2/PtCu nanoconjugates. The appearance of characteristic absorption bands for -NH, -CH_2 and phosphodiester bond in FTIR spectra and the considerable decrease in the zeta-potential also indicated the successful modification of aptamers on MoS_2/PtCu.

Like oxidase and other nanomaterials-based oxidase mimics, the catalytic activity of the prepared nanoconjugates was also dependent on pH, temperature, and the concentration of substrates and catalyst (Fig. 4). For the catalytic oxidation of TMB by using apt-MoS_2/PtCu, the optimal pH is 3.5. The nanoconjugates exhibited good stability and high oxidase-like activity over a broad temperature range (30-60 ^oC). It was also found that the reaction speed depended on the catalyst concentration with excess reactants. To get the optimal colormetric signal for detection, the standard reaction were carried out at 30 ^oC by using 1 μg apt-MoS_2/PtCu in 1 mL of 20 mM

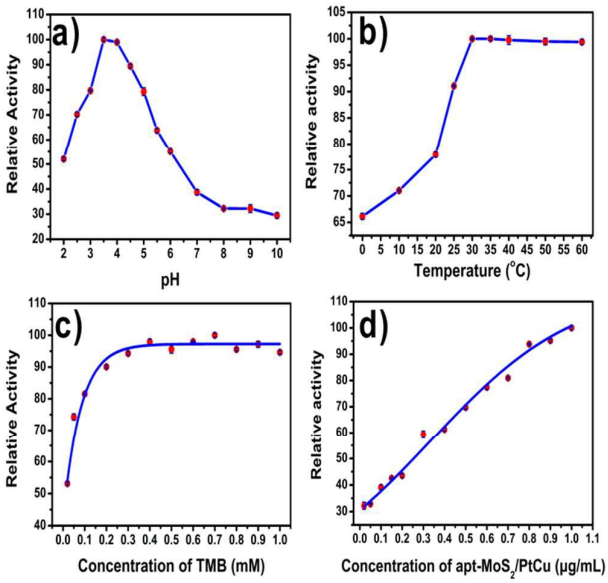

Fig. 4 Dependence of the oxidase-like activity of apt-MoS_2/PtCu on (a) pH, (b) temperature, (c) TMB concentration and (d) apt-MoS_2/PtCu nanocomposite concentration.

phosphate buffer solution (pH 3.5) with 10 μL TMB (0.4 mM) as the substrate.

By taking advantage of the oxides-like activity, selective binding apt-MoS_2/PtCu on the tumor cells can convert the recognition process into quantitative colorimetric signal (as shown in Scheme 1). For the colorimetric detection of cancer cells, it was first studied whether S2.2 aptamer functionalized MoS_2/PtCu (apt-MoS_2/PtCu) could efficiently differentiate between target cells and control cells. In this study, two MUC1 negative cell lines (HEK293 and HepG2)[56-58] and two MUC1 overexpressed cell lines (MCF-7 and A549)[57-61] were employed as control groups and target cells respectively.

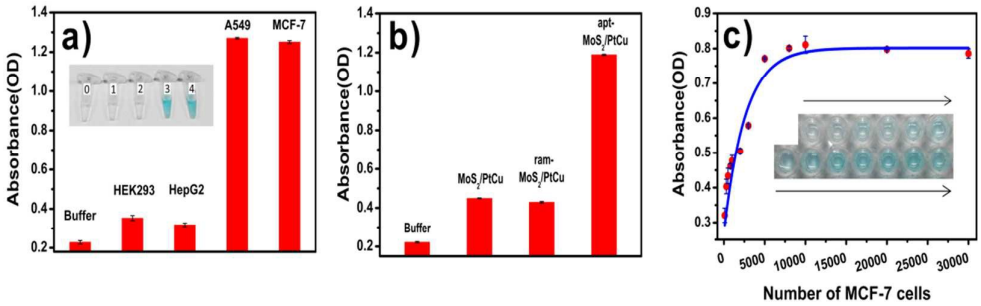

Fig. 5 (a) Response of different cells using apt-MoS_2/PtCu to TMB. (b) Colorimetric response of MCF-7 after incubation with different nanoconjugates (i: no nanoconjugates; ii: MoS_2/PtCu; iii: ram-MoS_2/PtCu; iv: apt-MoS_2/PtCu). (c) The absorption values at 652 nm after incubation with apt-MoS_2/PtCu depend on the number of MCF-7 cells.

As shown in Fig. 5a, an obvious difference of absorbance was observed between target cells and control cells, which suggested that apt-MoS_2/PtCu could bind selectively to MUC1 overexpressed cells (MCF-7 and A549) and catalyze a color change reaction in the presence of TMB. The above results also indicated that the nanoconjugates could give specific response to cancer cells with different level of MUC1-protein expression.

To further demonstrate the selectivity to target cells through the interaction between MUC1 proteins and S2.2 aptamers, random DNA modified MoS_2/PtCu nanoconjugates (ram-MoS_2/PtCu) was prepared and free S2.2 aptamers were used to locate the binding sites. The four samples are as follow: MCF-7 cells only, 0.2 μg MoS_2/PtCu with MCF-7 cells, 0.2 μg ram-MoS_2/PtCu with MCF-7 cells, and 0.2 μg apt-MoS_2/PtCu with MCF-7 cells. As a result (Fig. 5b), the absorbance of apt-MoS_2/PtCu with MCF-7 cells was significantly higher than the same amount of MoS_2/PtCu with MCF-7 cells and the same amount of ram-MoS_2/PtCu with MCF-7 cells, which suggested that apt-MoS_2/PtCu show much stronger binding ability to MCF-7 cells than MoS_2/PtCu and ram-MoS_2/PtCu. In addition, MCF-7 cells pretreated with free S2.2 aptamers showed a marked decrease in the absorbance, given that the binding of apt-MoS_2/PtCu to cells was blocked by S2.2 aptamers (Fig. S8). The corresponding results could also be observed visually from the images shown in Fig. S9. Consequently, the above results could demonstrate that the selective bound of apt-MoS_2/PtCu to targets cells was indeed through the interaction between MUC1 proteins of target cells and S2.2 aptamers. The proposed method might be generalized for cancer-cell detection.

The nanoconjugates were then used for quantitative colorimetric detection of MUC1 overexpressed cells (MCF-7). An increasing number of MCF-7 cells were incubated with a constant amount of apt-MoS_2/PtCu in PBS containing 0.5 % BSA for 1 h and subsequently washed. In the presence of TMB, the apt-MoS_2/PtCu conjugated cells catalyzed a color reaction that could be judged by the naked eye easily and be quantitatively monitored by the absorbance change at 652 nm. The results were shown in Fig. 5c. As the number of target cells increased, the absorbance at 652 nm changed rapidly, suggested that the increasing number of target cells translates into an increasing number of MUC1 proteins available for binding to apt-MoS_2/PtCu nanoconjugates. Using this method, as low as 300 MCF-7 cells could be detected, demonstrating good sensitivity of the method.

Conclusion

In summary, we have successfully prepared novel MoS_2/PtCu nanocomposites with excellent oxidase-like activity. As a mimic oxidase, MoS_2/PtCu nanocomposites show several advantages over natural enzymes and other existing alternatives. First, MoS_2/PtCu

can be prepared easily in a short time and have high stability against aggregation. Second, the employment of MoS_2 nanosheets as an ideal carrier improves the catalytic activity and leads to be ease of functional modification and effective absorption of modifiers or drugs. Furthermore, the oxidation of substrates is independent of hydrogen peroxide, introducing better biocompatibility for promising biosensor applications. By taking advantage of MUC1 aptamer conjugated MoS_2/PtCu, we develop a sensitive and selective colorimetric aptasensor for cancer-cell detection based on the oxides-like activity of MoS_2/PtCu nanocomposites. As the preparation processes of the proposed aptasensor are easy and time-saving, our work will facilitate the utilization of MoS_2/PtCu with intrinstic oxidase activity in bioassays and biotechnology by altering different recognition elements with the practical demands, such as aptamers, nuclei acids, antibodies and peptides.

Experimental Section

Preparation of MoS_2/PtCu nanocomposites

Chitosan-modified single-layer MoS_2 nanosheets were produced by a modified oleum treatment exfoliation process.[62] For a typical synthesis of MoS_2/PtCu nanocomposites, 3 mL (25 mg/L) MoS_2 nanosheet aqueous dispersion was mixed with 23.3 μL H_2PtCl_6 aqueous solution (19.3 mM) and 7.5 μL $Cu(OAc)_2$ aqueous solution (20 mM). The mixture was stirred in an ice-water bath at 0°C for 15 min. Then，$NaBH_4$ (10.5 mM, 1 mL) aqueous solution was dropwise added into the mixture under vigorous stirring. The addition time of $NaBH_4$ was 30min. After the reaction of 2 h, the resulting solution was centrifuged and washed by water. The obtained precipitate was re-dispersed in water before further characterization or modification.

Characterization

Transmission electron microscopy (TEM) images of MoS_2/PtCu were obtained by a transmission electron microscope (FEI Tecnai G2 20 S-TWIN) operating at an accelerating voltage of 200 kV. High resolution TEM (HR-TEM) images were obtained by a high-resolution transmission electron microscopy (HRTEM, FEI Tecnai G2 F20 U-TWIN). The crystalline structure of the nanocomposites was determined using a X-ray powder diffractometer (XRD, Bruker D8 focus) with Cu Kα radiation (l= 1.5406 Å) at room temperature. X-ray photoelectron spectra (XPS) were measured using an X-ray photoelectron spectrometer (Thermo Fisher ESCALAB 250Xi). The composition of the products was determined by the inductively coupled plasma optical emission spectrometer (ICP-OES, Thermo Scientific iCAP 6300). Zeta potential data was obtained using a nanoparticle analyzer (Malvern Zetasizer Nano ZS). FT-IR spectra were recorded on PerkinElmer Spectrum One FT-IR spectrometer in the transmission mode using CaF_2.

Enzyme-like activity of MoS_2/PtCu nanocomposites

To investigate the oxidase-like activity of MoS_2/PtCu nanocomposites, the reaction was carried out at 30 ^oC by using 1μg MoS_2/PtCu in 1 mL of 20 mM phosphate buffer solution (pH 3.5) with 10 μL TMB (0.4 mM) as the substrate. The absorption spectra were collected on a 96-well plate in Molecular Devices Spectramax M5 microplate reader.

To investigate the apparent kinetic parameters, assays were carried out under standard reaction conditions as described above by varying concentrations of TMB with a fixed concentration of H_2O_2 or vice versa. The apparent kinetic parameters were calculated based on the function $v = V_{max} \times [S] / (K_m + [S])$, where v is the initial velocity, V_{max} is the maximal reaction velocity, [S] is the concentration of the substrate and K_m is the Michaelis constant.

Modification of MoS_2/PtCu nanocomposites with S2.2 aptamers

MoS_2/PtCu nanocomposite dispersion was mixed with streptavidin aqueous solution (1.5 μM) at first. The mixture was incubated at room temperature for 5 h with shaking. Then streptavidin was adsorbed onto MoS_2/PtCu nanocomposites. Unbound streptavidin was removed by centrifugation and repeatedly washing the sample with water. The resulting stv-MoS_2/PtCu was re-dispersed in water and then incubated with biotinylated S2.2 aptamer (2 μM) at room temperature for 1 h. Unbound aptamers were removed by centrifugation. The obtained apt-MoS_2/PtCu were re-dispersed in PBS after washing twice and stored at 4 ^oC.

Cell culture and treatment

The human breast cancer cells (MCF-7), human liver carcinoma cells (Hep G2) and human embryonic kidney 293 cells (HEK 293) were cultured in Dulbecco's modified Eagle's medium (Corning) supplemented with 10 % fetal bovine serum in a humidified 37 ^oC incubator with 5 % CO_2. The human lung adenocarcinoma cells (A549) were cultured in F-12K medium

(Corning) supplemented with 10 % fetal calf serum. For cell assay, 1 μg/mL apt-MoS_2/PtCu nanocomposites were incubated with different cell lines in 200 μL PBS containing 0.5 % BSA for 1 h at room temperature and then centrifuged. The precipitates were washed three times with PBS and then 150 μL 0.4 mM TMB was added. The samples were incubated in phosphate buffer (pH 3.5) for 20 min to allow development of the blue color. The absorbance of the oxidation product was monitored at 652 nm with a microplate reader.

Acknowledgements

This work was supported by National Natural Science Foundation of China (21405027, 21573050 and 21501034) and Chinese Academy of Sciences (XDA09030303). Financial support from CAS Key Laboratory of Biological Effects of Nanomaterials and Nanosafety is also gratefully acknowledged.

Notes and references

1 C. Burda, X. B. Chen, R. Narayanan and M. A. El-Sayed, *Chem. Rev.*, 2005, **105**, 1025-1102.
2 A. Roucoux, J. Schulz and H. Patin, *Chem. Rev.*, 2002, **102**, 3757-3778.
3 L. Z. Gao, J. Zhuang, L. Nie, J. B. Zhang, Y. Zhang, N. Gu, T. H. Wang, J. Feng, D. L. Yang, S. Perrett and X. Yan, *Nat. Nanotechnol.*, 2007, **2**, 577-583.
4 R. Andre, F. Natalio, M. Humanes, J. Leppin, K. Heinze, R. Wever, H. C. Schroder, W. E. G. Muller and W. Tremel, *Adv. Funct. Mater.*, 2011, **21**, 501-509.
5 A. Asati, S. Santra, C. Kaittanis, S. Nath and J. M. Perez, *Angew. Chem. Int. Edit.*, 2009, **48**, 2308-2312.
6 W. Luo, Y. S. Li, J. Yuan, L. H. Zhu, Z. D. Liu, H. Q. Tang and S. S. Liu, *Talanta*, 2010, **81**, 901-907.
7 W. B. Shi, X. D. Zhang, S. H. He and Y. M. Huang, *Chem. Commun.*, 2011, **47**, 10785-10787.
8 L. Su, J. Feng, X. M. Zhou, C. L. Ren, H. H. Li and X. G. Chen, *Anal. Chem.*, 2012, **84**, 5753-5758.
9 W. B. Shi, Q. L. Wang, Y. J. Long, Z. L. Cheng, S. H. Chen, H. Z. Zheng and Y. M. Huang, *Chem. Commun.*, 2011, **47**, 6695-6697.
10 H. X. Li and L. J. Rothberg, *J. Am. Chem. Soc.*, 2004, **126**, 10958-10961.
11 Y. J. Song, K. G. Qu, C. Zhao, J. S. Ren and X. G. Qu, *Adv. Mater.*, 2010, **22**, 2206-2210.
12 Q. J. Lu, J. H. Deng, Y. X. Hou, H. Y. Wang, H. T. Li and Y. Y. Zhang, *Chem.Commun.*, 2015, **51**, 12251-12253.
13 Q. Chen, M. L. Liu, J. N. Zhao, X. Peng, X. J. Chen, N. X. Mi, B. D. Yin, H. T. Li, Y. Y. Zhang and S. Z. Yao, *Chem.Commun.*, 2014, 50, 6771-6774.
14 Y. Jv, B. X. Li and R. Cao, *Chem. Commun.*, 2010, **46**, 8017-8019.
15 G. L. Wang, X. F. Xu, L. Qiu, Y. M. Dong, Z. J. Li and C. Zhang, *ACS Appl. Mater. Inter.*, 2014, **6**, 6434-6442.
16 J. Fan, J. J. Yin, B. Ning, X. C. Wu, Y. Hu, M. Ferrari, G. J. Anderson, J. Y. Wei, Y. L. Zhao and G. J. Nie, *Biomaterials*, 2011, **32**, 1611-1618.
17 X. Q. Huang, Y. J. Li, Y. Chen, E. B. Zhou, Y. X. Xu, H. L. Zhou, X. F. Duan and Y. Huang, *Angew. Chem. Int. Edit.*, 2013, **52**, 2520-2524.
18 W. W. He, X. C. Wu, J. B. Liu, X. N. Hu, K. Zhang, S. A. Hou, W. Y. Zhou and S. S. Xie, *Chem. Mater.*, 2010, **22**, 2988-2994.
19 W. W. He, Y. Liu, J. S. Yuan, J. J. Yin, X. C. Wu, X. N. Hu, K. Zhang, J. B. Liu, C. Y. Chen, Y. L. Ji and Y. T. Guo, *Biomaterials*, 2011, **32**, 1139-1147.
20 D. S. Wang and Y. D. Li, *Adv. Mater.*, 2011, **23**, 1044-1060.
21 W. T. Yu, M. D. Porosoff and J. G. G. Chen, *Chem. Rev.*, 2012, **112**, 5780-5817.
22 S. G. Ge, F. Liu, W. Y. Liu, M. Yan, X. R. Song and J. H. Yu, *Chem. Commun.*, 2014, **50**, 475-477.
23 L. H. Li, Y. Wu, J. Lu, C. Y. Nan and Y. D. Li, *Chem. Commun.*, 2013, **49**, 7486-7488.
24 J. Zhao, W. B. Hu, H. Q. Li, M. Ji, C. Z. Zhao, Z. B. Wang and H. Q. Hu, *RSC Adv.*, 2015, **5**, 7679-7686.
25 C. J. Shearer, A. Cherevan and D. Eder, *Adv. Mater.*, 2014, **26**, 2295-2318.
26 Y. Hou, Z. H. Wen, S. M. Cui, S. Q. Ci, S. Mao and J. H. Chen, *Adv. Funct. Mater.*, 2015, **25**, 872-882.
27 Y. J. Guo, L. Deng, J. Li, S. J. Guo, E. K. Wang and S. J. Dong, *ACS Nano*, 2011, **5**, 1282-1290.
28 Y. J. Song, Y. Chen, L. Y. Feng, J. S. Ren and X. G. Qu, *Chem. Commun.*, 2011, **47**, 4436-4438.
29 X. L. Zuo, C. Peng, Q. Huang, S. P. Song, L. H. Wang, D. Li and C. H. Fan, *Nano Res.*, 2009, **2**, 617-623.
30 Y. L. Dong, H. G. Zhang, Z. U. Rahman, L. Su, X. J. Chen, J. Hu and X. G. Chen, *Nanoscale*, 2012, **4**, 3969-3976.
31 Y. Tao, Y. H. Lin, Z. Z. Huang, J. S. Ren and X. G. Qu, *Adv. Mater.*, 2013, **25**, 2594-2599.
32 L. N. Zhang, H. H. Deng, F. L. Lin, X. W. Xu, S. H. Weng, A. L. Liu, X. H. Lin, X. H. Xia and W. Chen, *Anal. Chem.*, 2014, **86**, 2711-2718.
33 B. Radisavljevic, A. Radenovic, J. Brivio, V. Giacometti and A. Kis, *Nat. Nanotechnol.*, 2011, **6**, 147-150.
34 V. K. Sangwan, H. N. Arnold, D. Jariwala, T. J. Marks, L. J. Lauhon and M. C. Hersam, *Nano Lett.*, 2013, **13**, 4351-4355.
35 Z. Y. Zeng, Z. Y. Yin, X. Huang, H. Li, Q. Y. He, G. Lu, F. Boey and H. Zhang, *Angew. Chem. Int. Edit.*, 2011, **50**, 11093-11097.
36 L. C. Yang, S. N. Wang, J. J. Mao, J. W. Deng, Q. S. Gao, Y. Tang and O. G. Schmidt, *Adv. Mater.*, 2013, **25**, 1180-1184.
37 T. T. Jia, A. Kolpin, C. S. Ma, R. C. T. Chan, W. M. Kwok and S. C. E. Tsang, *Chem. Commun.*, 2014, **50**, 1185-1188.
38 Q. J. Xiang, J. G. Yu and M. Jaroniec, *J. Am. Chem. Soc.*, 2012, **134**, 6575-6578.
39 S. E. Skrabalak and K. S. Suslick, *J. Am. Chem. Soc.*, 2005, **127**, 9990-9991.
40 N. Li, Y. M. Chai, B. Dong, B. Liu, H. L. Guo and C. G. Liu, *Mater. Lett.*, 2012, **88**, 112-115.
41 Z. H. Zhou, Y. L. Lin, P. A. Zhang, E. Ashalley, M. Shafa, H. D. Li, J. Wu and Z. M. Wang, *Mater. Lett.*, 2014, **131**, 122-124.
42 W. H. Liu, S. L. He, T. Yang, Y. Teng, G. Qian, J. Z. Xu and S. D. Miao, *Appl. Surf. Sci.*, 2014, **313**, 498-503.

43 T. R. Lin, L. S. Zhong, L. Q. Guo, F. F. Fu and G. N. Chen, *Nanoscale*, 2014, **6**, 11856-11862.
44 X. R. Guo, Y. Wang, F. Y. Wu, Y. N. Ni and S. Kokot, *Analyst*, 2015, **140**, 1119-1126.
45 B. L. Li, H. Q. Luo, J. L. Lei and N. B. Li, *RSC Adv.*, 2014, **4**, 24256-24262.
46 X. Hong, J. Q. Liu, B. Zheng, X. Huang, X. Zhang, C. L. Tan, J. Z. Chen, Z. X. Fan and H. Zhang, *Adv. Mater.*, 2014, **26**, 6250-6254.
47 T. S. Sreeprasad, P. Nguyen, N. Kim and V. Berry, *Nano Lett.*, 2013, **13**, 4434-4441.
48 L. Pan, Y. T. Liu, X. M. Xie and X. D. Zhu, *Chem.-Asian J.*, 2014, **9**, 1519-1524.
49 L. H. Yuwen, F. Xu, B. Xue, Z. M. Luo, Q. Zhang, B. Q. Bao, S. Su, L. X. Weng, W. Huang and L. H. Wang, *Nanoscale*, 2014, **6**, 5762-5769.
50 K. Ishibashi, A. Fujishima, T. Watanabe and K. Hashimoto, *J. Photoch. Photobio. A*, 2000, **134**, 139-142.
51 A. I. Mitsionis and T. C. Vaimakis, *J. Therm. Anal. Calorim.*, 2013, **112**, 621-628.
52 C. S. M. Ferreira, C. S. Matthews and S. Missailidis, *Tumor Biol.*, 2006, **27**, 289-301.
53 C. S. M. Ferreira, M. C. Cheung, S. Missailidis, S. Bisland and J. Gariepy, *Nucleic Acids Res.*, 2009, **37**, 866-876.
54 T. M. Horm and J. A. Schroeder, *Cell Adhes. Migr.*, 2013, **7**, 187-198.
55 J. L. Deng, L. Wang, H. M. Chen, L. Li, Y. M. Ma, J. Ni and Y. Li, *Cancer Metast. Rev.*, 2013, **32**, 535-551.
56 S. Mahanta, S. P. Fessler, J. Park and C. Bamdad, *PLoS One*, 2008, **3**, e2054.
57 Y. Hu, J. H. Duan, Q. M. Zhan, F. D. Wang, X. Lu and X. D. Yang, *PLoS One*, 2012, **7**, e31970.
58 X. H. Wang, Q. S. Han, N. Yu, J. Y. Li, L. Yang, R. Yang and C. Wang, *J. Mater. Chem. B*, 2015, **3**, 4036-4042.
59 L. F. Ren, M. A. Marquardt and J. J. Lech, *Chem.-Biol. Interact.*, 1997, **104**, 55-64.
60 M. V. Croce, A. G. Colussi, M. R. Price and A. Segal-Eiras, *Pathology oncology research : POR*, 1999, **5**, 197-204.
61 M. V. Croce, M. T. Isla-Larrain, A. Capafons, M. R. Price and A. Segal-Eiras, *Breast Cancer Res. Tr.*, 2001, **69**, 1-11.
62 W. Y. Yin, L. Yan, J. Yu, G. Tian, L. J. Zhou, X. P. Zheng, X. Zhang, Y. Yong, J. Li, Z. J. Gu and Y. L. Zhao, *ACS Nano*, 2014, **8**, 6922-6933.

Enhanced Oxidase/peroxidase-like Activities of Aptamer Conjugated MoS_2/PtCu Nanocomposites and Their Biosensing Application

Cui Qi[†], Shuangfei Cai[†], Xinhuan Wang, Jingying Li, Zheng Lian, Shanshan Sun, Rong Yang* and Chen Wang*

Taking advantage of bimetallic alloy nanoparticles and MoS_2 nanosheets, a colorimetric aptasensor was developed for MUC1 overexpressed cancer cell detection.